journal

J. Am. Ceram. Soc., **99** [11] 3802–3808 (2016)
DOI: 10.1111/jace.14397

Formation and Accumulation of Intragranular Pores in the Hydrothermally Synthesized Barium Titanate Nanoparticles

Changyeon Baek,[‡] Ji Eun Wang,[‡] San Moon,[‡,§§] Chang-Hak Choi,[§] and Do Kyung Kim[‡,†,*]

[‡]Department of Materials Science and Engineering, KAIST, Yuseong-gu, Daejeon 34141, Korea

[§]LCR Material Development Group, Samsung Electro-Mechanics, Suwon 16674, Korea

As highly integrated circuits are demanded for high-performance electric devices, small sizes of barium titanate ($BaTiO_3$) as a dielectric material are desirable for the application of multilayer ceramic capacitors. Since the small sizes of the particles degrade the dielectric property, especially below a certain critical size, understanding the probable cause is significant for the high-performance capacitors. Here, we have demonstrated nanosized $BaTiO_3$ with average size below 30 nm and a uniform size distribution. High-resolution transmission electron microscopy (TEM) shows that the as-synthesized $BaTiO_3$ contains intragranular pores. We have analyzed the correlation between the intragranular pores inside nanoparticles and their phase ratio of cubic and tetragonal. We have found that the presence of the intragranular pores affects low tetragonality of $BaTiO_3$ particles, and the intragranular pores are generated by the accumulation of hydroxyl groups during hydrothermal reaction. Formation and accumulation of intragranular pores have been investigated by ex-situ synchrotron X-ray diffraction and TEM analysis, suggesting the phase evolution model of nanosized $BaTiO_3$.

Keywords: *barium titanate; microstructure; hydrothermal; intragranular pores*

I. Introduction

Progress in synthesis methods for nanoscale materials accelerates the advance in miniaturization of various electronic applications. As mobile devices develop rapidly, highly integrated circuits are needed to achieve better performance at the same size. A multilayer ceramic capacitor (MLCC) is one of the essential components for every kind of electronic device. To maintain sufficient capacitance, even with a smaller size MLCC, the number of dielectric layers should be increased while the thickness of those layers is minimized. Among the perovskite oxides, barium titanate ($BaTiO_3$) is one of the promising candidates to satisfy this trend because of its prominent dielectric properties.[1,2] Due to their relatively biocompatible property compared with other lead-based perovskite ceramics, $BaTiO_3$ nanoparticles may also be employed in novel applications, including nanocomposite generators,[3] based on their piezoelectric properties and their biomarkers that exhibit second-harmonic generation behaviors.[4] All of these properties are attributed to spontaneous polarization based on the displacement of the Ti atom in the unit cell.

However, size-dependent property degradation of $BaTiO_3$ nanoparticles becomes a significant issue for downsizing.[5,6] It is generally accepted that the tetragonal phase in $BaTiO_3$ nanoparticles, which contributes to the dielectric property, decreases when their size becomes smaller. This happens for several reasons. One reason is the decrease of spontaneous polarization caused by lattice expansion. An *ab initio* study carried by S. Tsunekawa et al. explains that the interatomic distances of the Ba–Ti bond and the Ba–O bond are elongated by electrostatic repulsion as the number of atoms in a cluster decreases, resulting in the phase transition to a cubic structure.[7] This lattice relaxation mainly occurs on the surface of the particles. Zhu et al. directly observed the cubic surface layer in $BaTiO_3$ nanoparticles using high-resolution TEM.[8] As the particle size decreases, the surface portion increases significantly. Therefore, the overall crystal structure can change from tetragonal to cubic even at room temperature. This phase transition of $BaTiO_3$ nanoparticles has been extensively studied by many researchers. Hoshina et al. reported the size-induced phase transition behaviors of almost pore-free $BaTiO_3$ nanoparticles prepared by the two-step thermal decomposition of the barium titanyl oxalate precursor.[5] According to the report, the tetragonal to cubic phase transition was observed when the particle size was smaller than 30 nm. However, the critical size where the phase transition occurs still remains uncertain. Zhang et al. reported that 5 nm $BaTiO_3$ nanoparticles free of internal pores and synthesized via the glycothermal route still have very high tetragonal distortion.[9] Moreover, the coexistence of tetragonal and orthorhombic phases in 5 nm $BaTiO_3$ particles has also been reported.[10,11]

Another cause for the degradation of the dielectric property of $BaTiO_3$ particles is the presence of intragranular pores. A hydrothermal reaction has been used in the industry for the synthesis of $BaTiO_3$ particles, especially for the synthesis of the nano-sized particles because it allows for easy control of the size and shape, crystallization without calcination, and less agglomeration of the products. However, internal hydroxyl defects are generally captured in each $BaTiO_3$ particle during the hydrothermal reaction.[12] Although there are several reports that suggest the effects of hydroxyl defects on the phase transition and dielectric property change, they could not directly explain the phase change because of the distribution and size change of pores in similar-sized $BaTiO_3$ nanoparticles.[13–17]

Here, we investigate the tetragonal to cubic phase ratio change related to the presence of pores in synthesized $BaTiO_3$ particles with sizes below 30 nm via hydrothermal reaction. These small-sized particles enable easy observation of the internal pores by high-resolution TEM without any heat treatment. The changes in the internal pore sizes and distribution with reaction time are carefully measured. The changes in the proportion of the phases with the presence of pores are analyzed based on the Rietveld refinement of the synchrotron X-ray diffraction patterns of the synthesized nanoparticles.

R. Riman—contributing editor

Manuscript No. 37673. Received October 22, 2015; approved June 20, 2016.
[§§]Present address: Energy Lab., Samsung Advanced Institute of Technology, Suwon 16678, Korea.
*Fellow, The American Ceramic Society.
[†]Author to whom correspondence should be addressed. e-mail: dkkim@kaist.ac.kr

II. Experimental Procedure

(1) Synthesis of $BaTiO_3$ Nanoparticles

Two different samples were prepared to observe the change in particle size with the presence of the additives, diethylene glycol (DEG) [$(HOCH_2CH_2)_2O$, 99%, Sigma-Aldrich, Milwaukee, WI] and glycolic acid ($HOCH_2COOH$, technical grade, 70 wt% in H_2O, Sigma-Aldrich), as a function of the reaction time. The crystalline $BaTiO_3$ nanoparticles were synthesized by hydrothermal reaction using barium hydroxide monohydrate [$Ba(OH)_2{\cdot}H_2O$, 98%, Sigma-Aldrich] and Ti-butoxide ($Ti[O(CH_2)_3CH_3]_4$, reagent grade 97%, Sigma-Aldrich) as precursor materials. The mixture of Ti-butoxide (25 mmol), 5 mL of DEG, and 10 mL of high-purity ethanol was heated to 80°C under magnetic stirring in a water bath. The amorphous TiO_2 powder was precipitated by the addition of 4 mL of ammonia solution (25% NH_3 in H_2O, Sigma-Aldrich) to the mixture. Barium hydroxide (37.5 mmol) was dissolved in 10 mL of preheated deionized water in parallel (barium and titanium precursors in a 1.5 Ba/Ti molar ratio). The clear barium hydroxide aqueous solution was added to the TiO_2 precipitates, followed by the addition of 1 mL of glycolic acid. For the preparation of a control sample, the DEG and glycolic acid were not added and the other precursors and the reaction condition were fixed. The resultant suspension was stirred for an hour, then sealed in a 100 mL Teflon-lined stainless-steel autoclave with a fill factor of 70%. The hydrothermal reaction was conducted at 200°C for periods of time from 1 to 24 h under autogenous pressure. After the reaction, the autoclave was cooled to room temperature. The resultant powder was repeatedly washed using high-purity ethanol and deionized water, and subsequently dried at 80°C for 24 h in air.

(2) Characterization

The morphology of the particles was observed using field-emission scanning electron microscope (Model XL30, Philips, Amsterdam, the Netherlands) and field-emission transmission electron microscope (Tecnai G^2 F30 S-Twin, Eindhoven, the Netherlands). The particle sizes were measured by SEM and TEM images and using an image analysis program (*Image J*). The surface area of the synthesized particles was measured by the Brunauer–Emmett–Teller (BET) method (Tristar 3020, Micrometrics, Norcross, GA). Fourier-transform infrared spectroscopy (Model IFS66V/s & HYPERION, Bruker Optiks, Billerica, MA) data were obtained using the KBr pellet technique. Thermogravimetric analysis (TGA; Model TGA 92-18, Setaram, Caluire, France) of the synthesized $BaTiO_3$ powders was performed in air atmosphere with a temperature control from room temperature to 1000°C at a rate of 5°C/min.

The structures of the synthesized $BaTiO_3$ powders were investigated by X-ray diffraction [XRD; Rigaku D/Max-RB (12 KW), Tokyo, Japan] with CuK_α radiation (λ = 1.5148 Å) operating at 40 kV and 300 mA with a step size of 0.01° at $2°/min^{-1}$ in a 2-θ range from 20° to 80°. Synchrotron powder XRD data were collected at room temperature using a Beamline 9B (λ = 1.5474 Å) at Pohang Accelerator Laboratory in Pohang, Republic of Korea with a six multidetector system over a range between 10° and 130° at 0.02° step width. The obtained diffraction data were refined using the GSAS program with EXPGUI.[18]

The Raman spectra were obtained using a high-resolution dispersive Raman microscope (LabRAM HR UV/Vis/NIR, Horiba Jobin Yvon, Longjumeau, France). The measurements were conducted using the 514.5 nm line of an Ar^+ laser at room temperature. The Raman spectrum range from 100 to 1000 cm^{-1} was measured.

III. Results and Discussion

Significant size reduction was obtained via the addition of organic additives. Figures 1(a) and (b) show the SEM images and the size distribution of the synthesized $BaTiO_3$ nanopowders at 200°C for 24 h without and with organic additives. The average size (D_{SEM50} = 31.4 nm, D_{SEM99}/D_{SEM50} = 1.62) of $BaTiO_3$ synthesized in the presence of DEG and glycolic acid is approximately three times smaller than that (D_{SEM50} = 94.0 nm, D_{SEM99}/D_{SEM50} = 1.49) of $BaTiO_3$ synthesized without those additives. The monodispersed nanopowders have narrow size distribution (D_{SEM99}/D_{SEM50}) shown in Fig. 1(c), which is attributed to the presence of ammonia. In our recently published paper, we observed that the addition of ammonia solution promoted the uniformity of the synthesized powders by increasing the reaction sites of Ti-precursors with Ba^{2+}.[19]

Figure 1(d) shows the particle size change calculated using Eq. (1) from the BET surface area of the samples with different reaction times from 1 h up to 24 h. The graph reveals that the particle sizes prepared in the presence of organic additives were not noticeably changed after 4 h reaction while the sizes of the control samples increase continuously with reaction time.

$$D_{BET,nm} = \frac{6000}{\text{density} \times \text{BET surface area}\left(\frac{m^2}{g}\right)} \quad (1)$$

The calculated sizes by the above equation are well matched with the average sizes directly measured from the SEM images shown in the inset of Fig. 1(d). This implies that the synthesized particles maintain their surface boundaries without any open pores.

Figure 1(e) shows the infrared (IR) spectra of the synthesized nanopowders. The band around 3200–3700 cm^{-1} is related with the OH^- stretching vibration which represents both lattice and surface hydroxyl group. The bands at 1650 and 3560 cm^{-1} are also indicative characteristics of the H_2O molecule.[20] Two relatively weak absorption bands appear at 1040–1060 cm^{-1} and 1100 cm^{-1} in the IR result of the powder synthesized with additives, representing the presence of the primary and secondary alcoholic –CO bond, respectively. These bands would come from the DEG and the glycolic acid. There were no other noticeable peaks which represent the absorption of organic additives in IR spectra. It may be attributed to the relatively simple molecular structures of the additives. Compared to other glycols and carboxyl acids, glycolic acid and diethylene have shorter $–CH_2$ chains. Moreover, smaller amount of glycol and acid were added in this experiment than other reported papers which used glycol and carboxyl acid as a main reaction media.[9,21–24] Only small amount of absorbed organics would remain while most of organic additives were washed away during the washing with large amount of distilled water and ethanol mixture solution. From the TGA shown in Fig. 1(f), the presence of the surface absorbed water and the lattice hydroxyl group can be observed. The mass loss at the temperature range from room temperature to around 500°C was caused by not only evaporation of surface absorbed water but also decomposition of organic residue. The larger mass loss around 3.57 wt% in the nanopowder synthesized with additives attributes larger surface area. The weight change, which starts at the temperature around 700°C, can be attributed to the release of H_2O molecules from the intragranular pores which are resulted from the grain growth. The powder synthesized with additives shows larger mass loss than the powder synthesized without additives. This implies that the larger volume fraction of H_2O molecules was captured in the powder synthesized with additives. It resembles the previously reported pycnometry studies of the hydrothermally synthesized $BaTiO_3$ nanopowders in which a drastic increase of the density of powders was obtained at temperature near 700°C.[12,19] The mass loss around 0.5 wt% at temperature range from

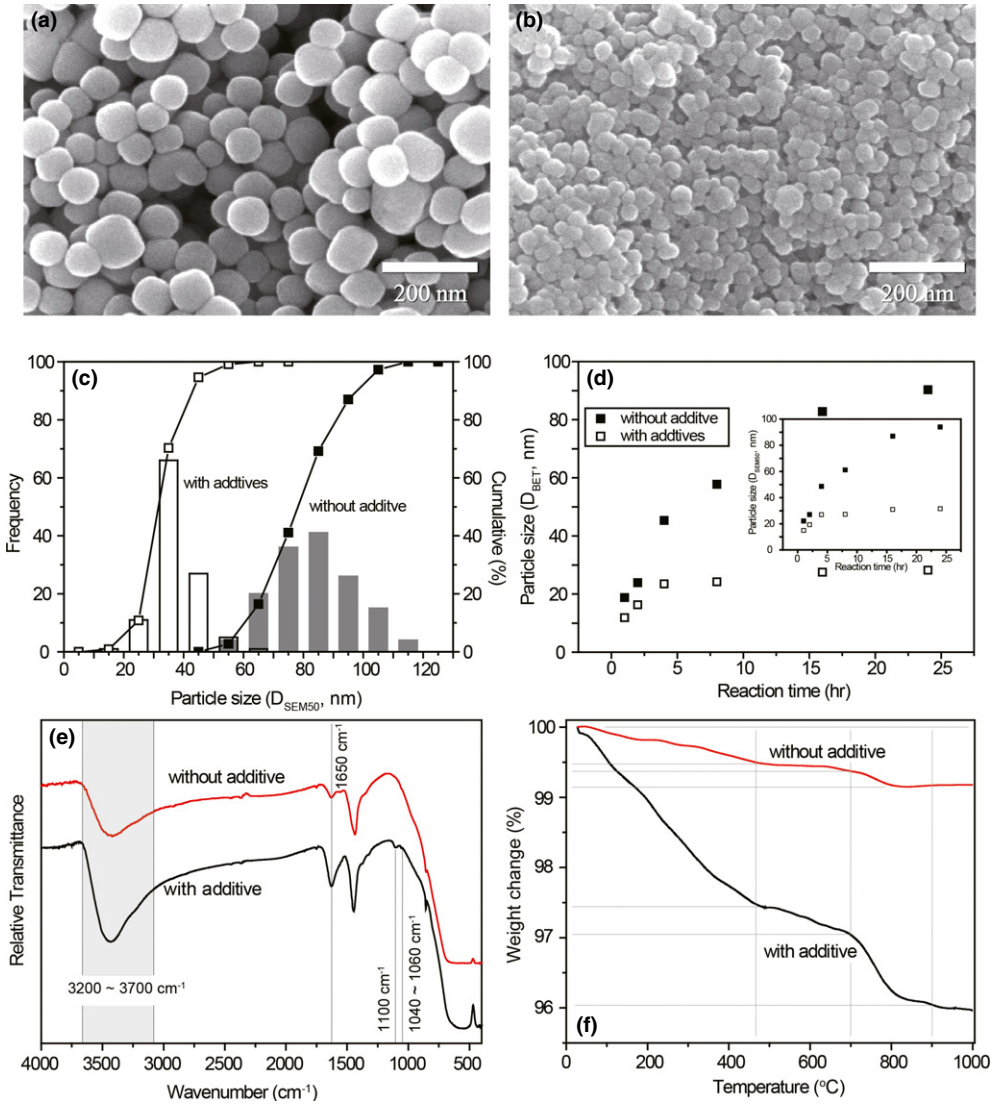

Fig. 1. SEM images of the synthesized $BaTiO_3$ nanopowder (a) without or (b) with additives at 200°C for 24 h. (c) Size distribution of the synthesized powders. (d) Particle size change with reaction time calculated based on the BET surface area results with inset of the measured particle size change from SEM images using the Image J program. (e) FT-IR spectrum and (f) thermogravimetric analysis of the synthesized powders.

500°C to 700°C was obtained in the synthesized powder with the additives while the powder synthesized without additives shows trivial weight change at this temperature range. The mass loss obtained from this region may represent the oxidation of the absorbed organic additives onto both the surface of particles. However, further study such as gas analysis during TGA is still needed to clarify the residual species in the synthesized powders. The significant difference in particle size change implies that the employed organic additives effectively suppress the particle growth. It is well-known that glycol[9,24,25] and carboxyl acid[22,23,26–28] are easily absorbed on the $BaTiO_3$ particle surface because of their hydrophilic nature. The absorbed glycol and carboxyl acid can control the particle growth by stabilizing the surface of the particles. Likewise, the employed DEG and glycolic acid act as a capping agent and assist in the separation of the initial $BaTiO_3$ precipitates by stabilizing the surface of the individual particles. This results in the apparent retardation of particle growth in the given condition. Therefore, crystal growth is controlled and suppressed during the reaction.

On the other hand, during the synthesis without organic additives, particles can be easily attached onto the other particles; therefore, particle growth occurs continuously from the initial $BaTiO_3$ particles geometrical disturbance.

The XRD patterns of the synthesized powders with organic additives at different reaction times are presented in Fig. 2(a). The diffraction peaks of the synthesized powder were placed between the cubic $BaTiO_3$ space group *Pm*3*m* (JCPDS No.31-0174) and the tetragonal $BaTiO_3$ space group *P*4*mm* (JCPDS No. 05-0626). Peak splitting between the (*h*00) and (00*l*) diffraction peaks does not appear in diffraction peaks from all samples. The maximum c/a ratio of tetragonal barium titanate is 1.011, which corresponds to δ $(c-a)/a = 1\%$. Therefore, the peaks converged into a single diffraction peak when the particles became nanosized, usually below 50 nm because of the peak broadening, even though the tetragonal phase existed in each particle. However, as seen in Fig. 2(b), slight peak shifts from the cubic to the tetragonal phase can be noticed.

It is also possible to identify the existence of the tetragonal phase in the synthesized particles by a spectroscopic technique, such as vibrational spectroscopy. The investigation of the tetragonal symmetry in $BaTiO_3$ by Raman spectroscopy has been extensively reported. It was well noted that the tetragonal $BaTiO_3$ shows Raman scattering modes of A_1(TO) at 250 cm^{-1}, [E(TO), A_1(LO)] at 520 cm^{-1}, [E(LO), A_1(LO)] at 720 cm^{-1} and [B_1, E(TO + LO)] at 307 cm^{-1}. The observed Raman spectra are consistent with those tetragonal

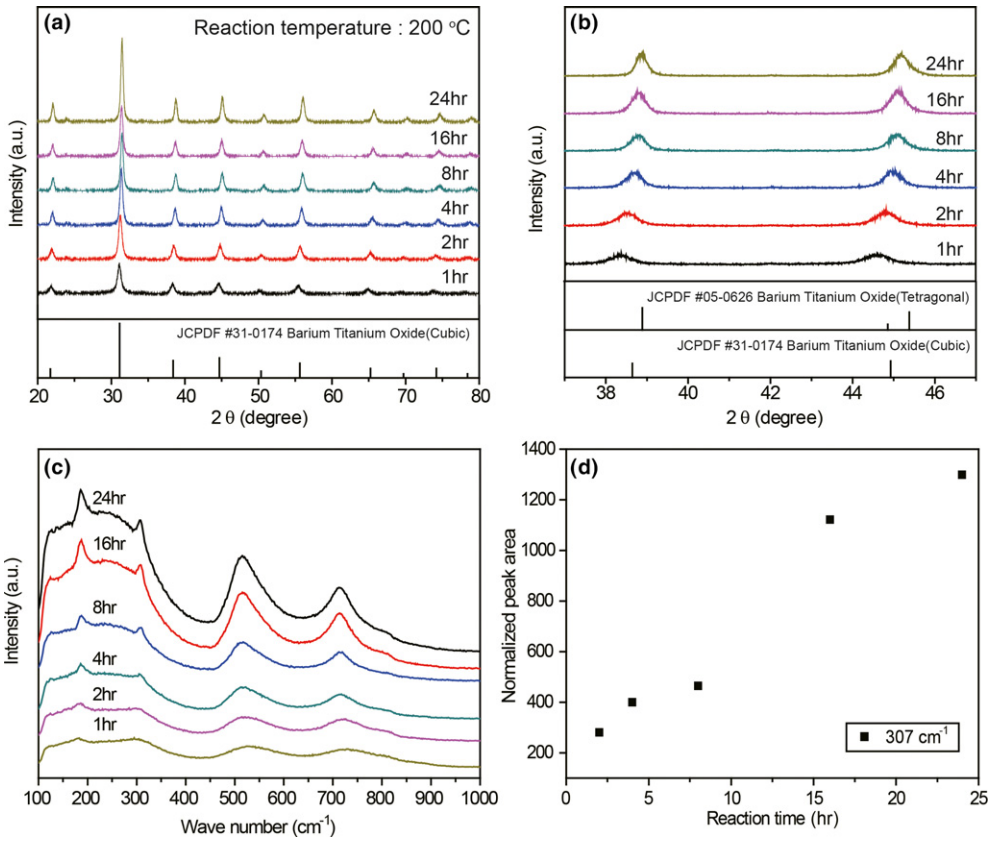

Fig. 2. Conventional laboratory XRD patterns [(a) 20°–80°, (b) 37°–47°] of $BaTiO_3$ samples synthesized at 200°C with different reaction times from 1 to 24 h. (c) Raman spectra of the same samples measured at room temperature. (d) Normalization of the Raman spectrum peak that appeared at 307 cm^{-1}.

modes. Taking account of the slightly appeared shoulder peak around 810 cm^{-1}, the lattice hydroxyl groups remain in the synthesized nanopowders.[15,29,30] According to the temperature-dependent characteristic of a sharp peak at 307 cm^{-1} reported by several researchers, the presence of the tetragonal phase in the $BaTiO_3$ crystal is closely related to this peak among all the other modes.[6,29,31,32] Therefore, we normalize the intensity of 307 cm^{-1} as a criteria for the presence of the tetragonal phase. Figure 2(c) shows the Raman spectra of the synthesized powders. The peak at approximately 307 cm^{-1} appears in the 4 hr-reacted powder prepared with organic additives. In Fig. 2(d), the normalized peak area obtained from the 307 cm^{-1} peak of the synthesized powders with organic additives increases with the reaction time. The changes in Raman spectroscopy and the X-ray diffraction peak shift imply that the tetragonal phase evolves in the synthesized powder.

For a more accurate investigation of the relative phase change, the synchrotron powder diffraction patterns of the synthesized powders were measured. The fitted profiles of the nanopowders obtained at different reaction times (2, 8, and 24 h) are shown in Fig. 3 and the corresponding Rietveld refinement results are summarized in Table I. Peak splitting does not appear even with high-energy X-ray diffraction, and the broadened peaks cannot be fitted suitably with a single phase. The synchrotron XRD patterns are fitted based on the conventional *Pm*3*m* cubic $BaTiO_3$ phase and the *P*4*mm* tetragonal $BaTiO_3$ phase. The impurity peaks of $BaCO_3$ were visible original XRD patterns of both Figs. 2 and 3. As a result, the impurity peaks are small enough that they are not evident in Fig. 2. In Fig. 3, which shows much higher resolution XRD results, the impurity peaks of $BaCO_3$ were evident. The resulting mol fractions of $BaCO_3$ phase were 6.2, 4.5, and 4.7 mol% for 2, 8, and 24 h powders. However, $BaCO_3$ impurity peaks are excluded to allow better calculation of the $BaTiO_3$ phases during Rietveld refinement process.

As shown in the insets of Fig. 3, with higher 2θ range (100°–125°), the obtained diffraction peaks are shifted to higher angles when the reaction time increases. The cubic cell parameter changes from $a = 4.0363$ Å ($V = 65.758$ Å^3) to $a = 4.0190$ Å ($V = 64.914$ Å^3) and the tetragonal lattice parameters also change from $a = 4.0233$ Å, $c = 4.0497$ Å ($V = 65.552$ Å^3) to $a = 4.0108$ Å, $c = 4.0312$ Å ($V = 64.846$ Å^3). This lattice expansion might originate in the increase of the cubic phase fraction. The cubic phase of 2 h-reacted nanopowder covers approximately 80% of each particle. However, the cubic to tetragonal ratio decreases with reaction time; finally, the tetragonal phase is evolved to approximately 70% in the 24 h-reacted particles. Taking account of the fractional change and the corresponding lattice parameter changes, the overall c/a ratio ($= a_{cubic}/a_{cubic} \times W_{cubic,\ \%} + c_{tetragonal}/a_{tetragonal} \times W_{tetragonal,\ \%}$ where W is weight percent of the phase) increases during first 8 h and rather stabilizes after 8 h.

At this point, it is worth discussing the evolution of the tetragonal phase in the particles synthesized with additives because the size of the particles was not significantly changed in this reaction time range. According to several reports, the amount of the tetragonal phase is closely related to the size of the particle.[5,6] The coexistence of the cubic and intermediate layer (gradient strain layer) with the tetragonal phase in individual particles lowers the portion of the tetragonal phase when the size of the particle decreases.[33,34] However, no report explained the reaction time-dependent tetragonal phase increase when the particle sizes remain almost the same, therefore, we focused on the presence of the internal pores. It is suggested that the point defects, which originated from the hydroxyl ions and proton ions are accumulated in order to compensate the large population of these ions which resides on lattices during the hydrothermal reaction resulting to form water molecules in the internal pores.[12] The presence of these intragranular pores in each particle, which can bring about a decrease in the tetragonal phase due to the material

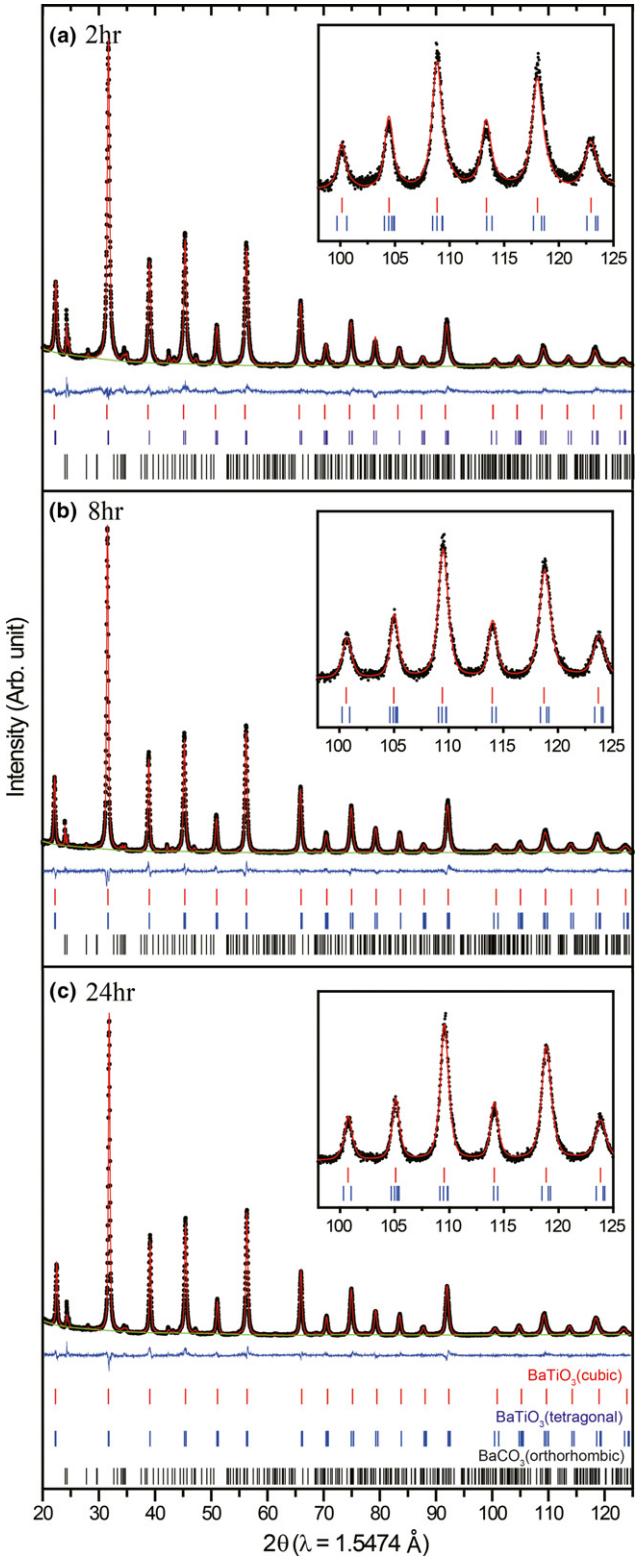

Fig. 3. Synchrotron XRD data and their fitted profiles for (a) 2, (b) 8, and (c) 24 h reacted $BaTiO_3$ nanoparticles. Dots (black) are observed data points, and the red lines are refined results. The difference curves (blue) and Bragg patterns of cubic and tetragonal $BaTiO_3$ are placed in order beneath the observed data. The impurity peaks ($BaCO_3$) were excluded during the refinement for the analysis of the $BaTiO_3$ cubic to tetragonal phase ratio.

deficiency from volumetric occupancy, should be considered along with the possibility of changes in the microstructure resulting from the lattice relaxation, which can be generated at the bonding ends.[35]

Figure 4(a) shows the TEM images of the particles synthesized with organic additives at different reaction times. Internal pores captured in approximately 30 nm-sized particles can be easily distinguished. Although there can be a greater number of pores that would be captured inside a particle, taking account of the three-dimensional morphology, only the projected pores shown in the TEM images are counted. Noticeable internal pore changes with reaction time are observed. More than 10 ($No._{aver}$ = 10.67) tiny pores with the size of D_{TEM50} = 2.54 nm are captured in the 2 h-reacted sample. As the reaction time increases, the size of the pores increases while the number of pores decreases. Finally, less than two ($No._{aver}$ = 1.47) pores with the size of D_{TEM50} = 4.95 nm remain in the 24 h-reacted sample. These size and distribution changes of the internal pores are plotted in Fig. 4(b). The noticeable factor is that the overall internal pore volume, which is calculated from each reaction time, does not change significantly. The inner pores shown in the TEM images had almost circular shape. Therefore, the shape of the inner pores was assumed to be spherical. Although three-dimensional analysis on the inner pores would be very ideal, effective, and even critical to identify the actual distribution of the pores, the three-dimensional analysis could not be carried out in this study. The volumes of inner pores were calculated based on the observed diameter and the numbers of the inner pores which were measured directly from the high-resolution TEM images. These changes of the internal pores were more possible to occur for the reduction of the interfacial energy built in between internal pores and particles than for the lowering of the surface energy by particle growth.

These changes in internal pores can also explain the cubic to tetragonal phase ratio change. Formation of the cubic shell layer is closely related to both the hydroxyl ion on an oxygen site and lattice expansion.[7,13,16,35] Hydroxyl groups at the boundaries of internal pores will also be incorporated with the oxygen site of the lattice near the pores. Therefore, we assume that the cubic layer is formed not only at the surface of particle but also around the internal pores. Assuming both particles and internal pores are spheres and the cubic layers are uniformly formed around the internal pores and the surface, the thickness of the cubic layer is calculated as approximately 1.4 nm from the refined cubic weight fraction in Table I. Figure 5(a) shows the volumetric changes of each phase with reaction time when the measured internal pore size and the uniform cubic layer are considered. The graph clearly shows the increase of the tetragonal phase with reaction time. The tetragonal volume is simply calculated using Eq. (2). As the particle size increases, the volume of the cubic layer at the surface increases. On the other hand, the volume of the cubic layer formed around the pores decreases as the interfacial area is decreased by the accumulation of pores. The pore volume does not change in this period of reaction time.

$$V_{\text{tetragonal}} = V_{\text{particle}} - (V_{\text{cubic,surface}} + V_{\text{cubic,defect}} + V_{\text{defect}} \quad (2)$$

A schematic pores change model, as shown in Fig. 5(b), which is drawn based on the calculated values, can easily explain the increase of the tetragonal region in the particles with reaction time. The tetragonal phase can exist only in the small volume between the surface and the pores, considering the number of internal pores and their distribution in a few hours for reacted $BaTiO_3$ nanoparticles. The possibility of building up the tetragonal phase would be increased when the size of pores become larger as a result of the accumulation of those internal pores. Consequently, the overall tetragonality (c/a ratio) can be changed depending on the distribution of internal pores even though the size of particles does not change significantly.

Table I. Rietveld Refinement Results of Synchrotron X-ray Diffraction Data (λ = 1.5474 Å)

		Reaction time		
		2 h	8 h	24 h
Cubic	a (Å)	4.0363(6)	4.0214(8)	4.0190(8)
	V (Å^3)	65.7578	65.0346	64.9144
Tetragonal	a (Å)	4.0233(5)	4.0123(2)	4.0108(1)
	c (Å)	4.0497(9)	4.0324(3)	4.0312(3)
	V (Å^3)	65.5523	64.9147	64.8463
Cubic/tetragonal fraction (wt%)		80.1/19.9	37.5/62.5	30.6/69.4
c/a ratio		1.0013	1.0031	1.0035
$R_p/R_{wp}/R(F^2)$ (%)		0.057/0.074/7.14	0.057/0.074/3.38	0.077/0.077/5.43
χ^2		3.65	2.41	3.33

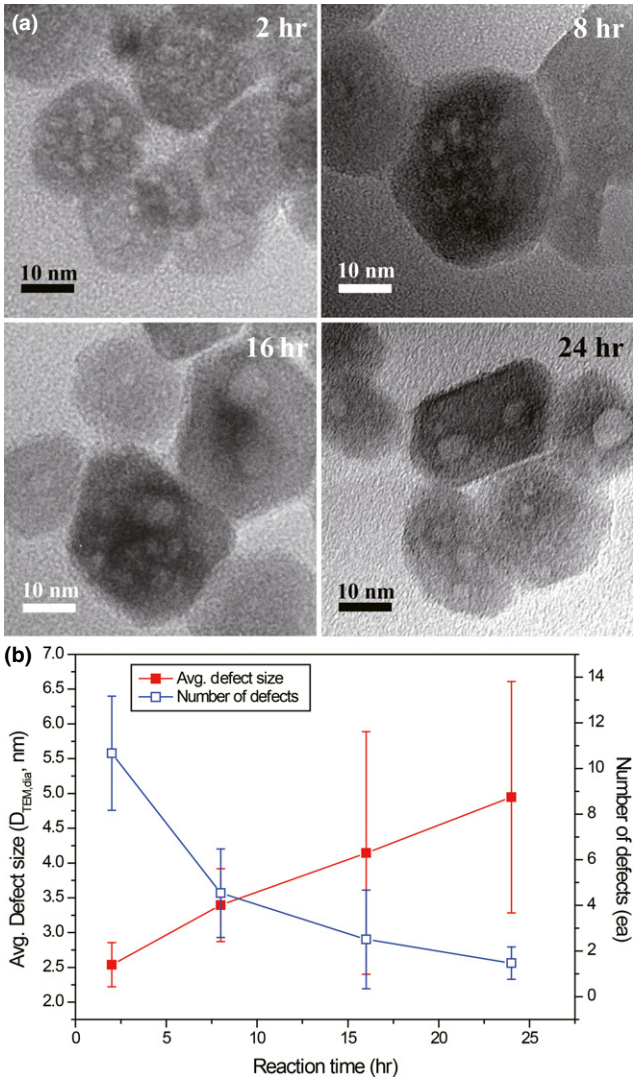

Fig. 4. Observation of internal defect changes (a) TEM images of the synthesized $BaTiO_3$ nanoparticles with additives. (b) Average defect size ($D_{TEM50,2\ h}$ = 2.54 nm→$D_{TEM50,24\ h}$ = 4.95 nm) and the number of defects (No.$_{aver,2\ h}$ = 10.67 ea→No.$_{aver,24\ h}$ = 1.47 ea) change as a function of the reaction time.

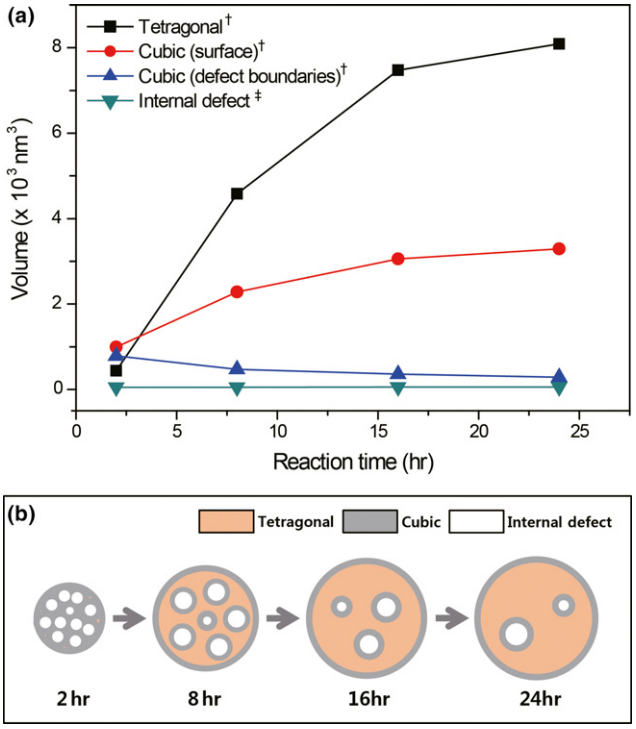

Fig. 5. (a) Volumetric phase change with reaction time calculated based on the Rietveld refinement results of synchrotron XRD data† and the directly measured sizes from TEM images, ‡Cubic layer formation with uniform thickness both at the surface and at the defect boundaries is assumed. (b) schematic phase evolution model corresponding to the internal defect changes.

IV. Conclusions

$BaTiO_3$ nanoparticles with a size below 30 nm have been synthesized with the addition of glycol and carboxyl acid. We suggest that the intragranular porosity changes depending on the reaction time in the synthesized $BaTiO_3$ nanoparticles, which has been observed by high-resolution TEM. The formation of intragranular pores has been attributed to the presence of hydroxyl groups. The Raman spectroscopy and Rietveld refinement of synchrotron X-ray diffraction patterns present the cubic to tetragonal phase ratio change in the similar-sized $BaTiO_3$ nanoparticles. The change in the cubic to tetragonal phase ratio has been considered to the size and distribution of intragranular pores. This study could potentially throw light on the probable causes of the low dielectric property when nanosized $BaTiO_3$ below the average sizes of 30 nm is used in MLCC.

Acknowledgments

This work was supported by the Program to Solve Climate Changes (NRF-2010-C1AAA001-2010-0029031) through the National Research Foundation of Korea (NRF) funded by the Ministry of Science, ICT & Future Planning. The authors thank the Pohang Accelerator Laboratory (PAL), the 9B-HRPD beamline, Korea for extending the synchrotron XRD for characterization.

References

[1]L. E. Cross, "Dielectric, Piezoelectric, and Ferroelectric Components," *Am. Ceram. Soc. Bull.*, **63** [4] 586–90 (1984).

[2]D. Hennings, M. Klee, and R. Waser, "Advanced Dielectrics - Bulk Ceramics and Thin-Films," *Adv. Mater.*, **3** [7–8] 334–40 (1991).

[3]K. I. Park, M. Lee, Y. Liu, S. Moon, G. T. Hwang, et al., "Flexible Nanocomposite Generator Made of $BaTiO_3$ Nanoparticles and Graphitic Carbons," *Adv. Mater.*, **24** [22] 2999–3004 (2012).

[4]C. L. Hsieh, R. Grange, Y. Pu, and D. Psaltis, "Three-Dimensional Harmonic Holographic Microcopy Using Nanoparticles as Probes for Cell Imaging," *Opt. Express*, **17** [4] 2880–91 (2009).

[5]T. Hoshina, H. Kakemoto, T. Tsurumi, S. Wada, and M. Yashima, "Size and Temperature Induced Phase Transition Behaviors of Barium Titanate Nanoparticles," *J. Appl. Phys.*, **99** [5] 054311 (2006).

[6]M. B. Smith, K. Page, T. Siegrist, P. L. Redmond, E. C. Walter, et al., "Crystal Structure and the Paraelectric-to-Ferroelectric Phase Transition of Nanoscale $BaTiO_3$," *J. Am. Chem. Soc.*, **130** [22] 6955–63 (2008).

[7]S. Tsunekawa, K. Ishikawa, Z. Q. Li, Y. Kawazoe, and A. Kasuya, "Origin of Anomalous Lattice Expansion in Oxide Nanoparticles," *Phys. Rev. Lett.*, **85** [16] 3440–3 (2000).

[8]X. H. Zhu, Z. G. Zhang, J. M. Zhu, S. H. Zhou, and Z. G. Liu, "Morphology and Atomic-Scale Surface Structure of Barium Titanate Nanocrystals Formed at Hydrothermal Conditions," *J. Cryst. Growth*, **311** [8] 2437–42 (2009).

[9]H. Zhang, X. H. Wang, Z. B. Tian, C. F. Zhong, Y. C. Zhang, et al., "Fabrication of Monodispersed 5-nm $BaTiO_3$ Nanocrystals with Narrow Size Distribution via One-Step Solvothermal Route," *J. Am. Ceram. Soc.*, **94** [10] 3220–2 (2011).

[10]W. Han, J. L. Zhu, S. J. Zhang, H. Zhang, X. H. Wang, et al., "Phase Transitions in Nanoparticles of $BaTiO_3$ as Functions of Temperature and Pressure," *J. Appl. Phys.*, **113** [19] 193513 (2013).

[11]Y. L. Li, Z. Y. Liao, F. Fang, X. H. Wang, L. T. Li, and J. Zhu, "Significant Increase of Curie Temperature in Nano-Scale $BaTiO_3$," *Appl. Phys. Lett.*, **105** [18] 182901 (2014).

[12]D. F. K. Hennings, C. Metzmacher, and B. S. Schreinemacher, "Defect Chemistry and Microstructure of Hydrothermal Barium Titanate," *J. Am. Ceram. Soc.*, **84** [1] 179–82 (2001).

[13]S. Wada, T. Suzuki, and T. Noma, "Preparation of Barium Titanate Fine Particles by Hydrothermal Method and Their Characterization," *J. Ceram. Soc. Jpn.*, **103** [12] 1220–7 (1995).

[14]S. Wada, T. Suzuki, and N. Tatsuo, "The Effect of the Particle Sizes and the Correlational Sizes of Dipoles Introduced by the Lattice-Defects on the Crystal-Structure of Barium-Titanate Fine Particles," *Jpn. J. Appl. Phys. 1*, **34** [9b] 5368–79 (1995).

[15]T. Noma, S. Wada, M. Yano, and T. Suzuki, "Analysis of Lattice Vibration in Fine Particles of Barium Titanate Single Crystal Including the Lattice Hydroxyl Group," *J. Appl. Phys.*, **80** [9] 5223–33 (1996).

[16]S. Wada, T. Suzuki, and T. Noma, "Role of Lattice Defects in the Size Effect of Barium Titanate Fine Particles–A New Model," *J. Ceram. Soc. Jpn.*, **104** [5] 383–92 (1996).

[17]R. Kota and B. I. Lee, "Effect of Lattice Hydroxyl on the Phase Transition and Dielectric Properties of Barium Titanate Particles," *J. Mater. Sci.-Mater. El*, **18** [12] 1221–7 (2007).

[18]B. H. Toby, "EXPGUI, a Graphical User Interface for GSAS," *J. Appl. Crystallogr.*, **34**, 210–3 (2001).

[19]S. Moon, H. W. Lee, C. H. Choi, and D. K. Kim, "Influence of Ammonia on Properties of Nanocrystalline Barium Titanate Particles Prepared by a Hydrothermal Method," *J. Am. Ceram. Soc.*, **95** [7] 2248–53 (2012).

[20]J. H. Park and S. Do Park, "Synthesis of Barium Titanate by Hydrothermal Method and Its Formation Mechanisms," *J. Chem. Eng. Jpn.*, **41** [7] 631–8 (2008).

[21]Y. J. Jung, D. Y. Lim, J. S. Nho, S. B. Cho, R. E. Riman, and B. W. Lee, "Glycothermal Synthesis and Characterization of Tetragonal Barium Titanate," *J. Cryst. Growth*, **274** [3–4] 638–52 (2005).

[22]P. F. Yu, B. Cui, and Q. Z. Shi, "Preparation and Characterization of $BaTiO_3$ Powders and Ceramics by Sol–Gel Process Using Oleic Acid as Surfactant," *Mater. Sci. Eng. a-Struct.*, **473** [1–2] 34–41 (2008).

[23]X. W. Yang, Y. W. Zeng, L. Q. Mo, and L. X. Han, "Oleic Acid Assisted Glycothermal Synthesis of Cuboidal $Ba_{0.6}Sr_{0.4}TiO_3$ Nanocrystals and Their Ordered Architectures via Self-Assembly," *J. Colloid Interface Sci.*, **357** [2] 308–16 (2011).

[24]Y. A. Hao, X. H. Wang, J. Kim, and L. T. Li, "Rapid Formation of Nanocrystalline $BaTiO_3$ and Its Highly Stable Sol," *J. Am. Ceram. Soc.*, **97** [11] 3434–41 (2014).

[25]H. Q. Zhan, X. F. Yang, C. M. Wang, J. Chen, Y. P. Wen, et al., "Multiple Nucleation and Crystal Growth of Barium Titanate," *Cryst. Growth Des.*, **12** [3] 1247–53 (2012).

[26]P. F. Yu, X. Wang, and B. Cui, "Preparation and Characterization of $BaTiO_3$ Powders and Ceramics by the Sol–Gel Process Using Organic Monoacid as Surfactant," *Scripta Mater.*, **57** [7] 623–6 (2007).

[27]B. Cui, P. F. Yu, and X. Wang, "Preparation and Characterization of $BaTiO_3$ Powders and Ceramics by Sol–Gel Process Using Decanedioic Acid," *J. Alloy. Compd.*, **459** [1–2] 589–93 (2008).

[28]S. Moon, C. H. Choi, C. Baek, and D. K. Kim, "The Effects of Propionic Acid on Nano-Sized $BaTiO_3$ Particles Synthesized by a Hydrothermal Method," *J. Nanosci. Nanotechnol.*, **14** [10] 8056–60 (2014).

[29]Y. Shiratori, C. Pithan, J. Dornseiffer, and R. Waser, "Raman Scattering Studies on Nanocrystalline $BaTiO_3$–Part I - Isolated Particles and Aggregates," *J. Raman Spectrosc.*, **38** [10] 1288–99 (2007).

[30]M. L. Moreira, G. P. Mambrini, D. P. Volanti, E. R. Leite, M. O. Orlandi, et al., "Hydrothermal Microwave: A New Route to Obtain Photoluminescent Crystalline $BaTiO_3$ Nanoparticles," *Chem. Mater.*, **20** [16] 5381–7 (2008).

[31]Y. Shiratori, C. Pithan, J. Dornseiffer, and R. Waser, "Raman Scattering Studies on Nanocrystalline $BaTiO_3$–Part II - Consolidated Polycrystalline Ceramics," *J. Raman Spectrosc.*, **38** [10] 1300–6 (2007).

[32]H. W. Lee, S. Moon, C. H. Choi, and D. K. Kim, "Synthesis and Size Control of Tetragonal Barium Titanate Nanopowders by Facile Solvothermal Method," *J. Am. Ceram. Soc.*, **95** [8] 2429–34 (2012).

[33]T. Hoshina, H. Kakemoto, T. Tsurumi, S. Wada, M. Yashima, et al., "Analysis of Composite Structures on Barium Titanate Fine Particles Using Synchrotron Radiation," *Key Eng. Mater.*, **301**, 239–42 (2006).

[34]T. Hoshina, S. Wada, Y. Kuroiwa, and T. Tsurumi, "Composite Structure and Size Effect of Barium Titanate Nanoparticles," *Appl. Phys. Lett.*, **93** [19] 192914 (2008).

[35]S. Tsunekawa, S. Ito, T. Mori, K. Ishikawa, Z. Q. Li, and Y. Kawazoe, "Critical Size and Anomalous Lattice Expansion in Nanocrystalline $BaTiO_3$ Particles (vol 62, art no 3065, 2000)," *Phys. Rev. B*, **67** [1] 3065–70 (2003). □